ACS APPLIED MATERIALS & INTERFACES

Research Article

Cite This: ACS Appl. Mater. Interfaces 2019, 11, 16647−16655

www.acsami.org

Tailoring Energy and Power Density through Controlling the Concentration of Oxygen Vacancies in V_2O_5/PEDOT Nanocable-Based Supercapacitors

Wenchao Bi,[†,‡] Evan Jahrman,[§] Gerald Seidler,[§] Jichao Wang,[⊥] Guohua Gao,[*,†] Guangming Wu,[*,†] Muhammad Atif,[∥] M. AlSalhi,[∥] and Guozhong Cao[*,‡]

[†]Shanghai Key Laboratory of Special Artificial Microstructure Materials and Technology, School of Physics Science and Engineering, Tongji University, Shanghai 200092, China

[‡]Department of Materials Science and Engineering, University of Washington, Seattle, Washington 98195-2120, United States

[§]Department of Physics, University of Washington, Seattle, Washington 98195-1560, United States

[⊥]Key Laboratory of Road and Traffic Engineering of the Ministry of Education, Tongji University, Shanghai 200092, China

[∥]Physics and Astronomy Department, College of Science, King Saud University, Riyadh 11451, Saudi Arabia

Supporting Information

ABSTRACT: Oxygen vacancies (Vö) play a crucial role in energy storage materials. Oxygen-vacancy-enriched vanadium pentoxide/poly(3,4-ethylenedioxythiophene) (Vö-V_2O_5/PEDOT) nanocables were prepared through the one-pot oxidative polymerization of PEDOT. PEDOT is used to create tunable concentrations of Vö in the surface layer of V_2O_5, which has been confirmed by X-ray absorption near edge structure (XANES) analysis and X-ray photoelectron spectroscopy (XPS) measurements. Applied as electrode materials for supercapacitors, the electrochemical performance of Vö-V_2O_5/PEDOT is improved by the synergistic effects of Vö in V_2O_5 cores and PEDOT shells with rapid charge transfer and fast Na^+ ion diffusion; however, it is compromised subsequently by excessive Vö in consuming more V^{5+} cations for Faradic reactions. Consequently, the specific capacitance and the energy density of Vö-V_2O_5/PEDOT nanocables are significantly enhanced when the overall concentration of Vö is 1.3%. The migration of Vö renders an increased capacitance (105% retention) after 10 000 cycles, which is verified and corroborated with density functional theory simulations and XANES analysis. This work provides an illumination for the fabrication of high-performance electrode materials in the energy storage field through Vö.

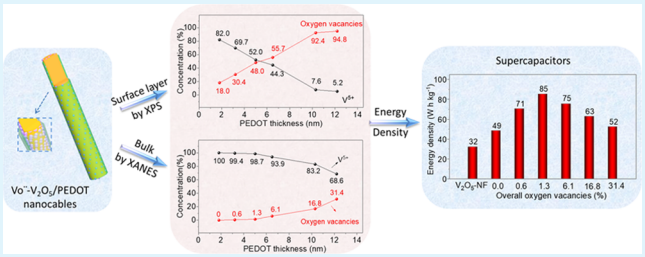

KEYWORDS: *V_2O_5, PEDOT, oxygen vacancies, tunable, supercapacitors*

INTRODUCTION

Supercapacitors, secondary batteries, and solar cell systems have attracted tremendous attention due to the ever-expanding demands for next-generation energy storage devices.[1−4] Supercapacitors appear as the most promising electrochemical energy storage devices for applications in portable electronic products and hybrid electric vehicles with the advantages of high-power delivery, expectant lifespan, and safety.[5−7] To date, extensive research studies have been focused on exploring suitable electrodes for satisfactory supercapacitors with high specific capacitance, energy density, and superior cyclability.[8−10] Carbonaceous materials such as graphene,[11] carbon fiber,[12] etc. are widely used as electrode materials for electric double layer capacitors due to fast ion adsorption/desorption. Conductive polymers (like polypyrrole,[13] polyaniline,[14] poly(3,4-ethylenedioxythiophene) (PEDOT),[15,16] etc.) and transition metal oxides (TMOs: RuO_2,[17] Co_3O_4,[18] V_2O_5,[19,20] etc.) are promising electrode materials in pseudocapacitors with fast Faradic reactions. TMOs have been extensively studied because of their high theoretical capacitances.[9,21] However, further application of TMO-based electrodes has been hampered by their low electrical conductivity and lack of cycling stability.[22] The delicate fabrication of high-energy and durable TMO electrode materials for supercapacitors is crucial but challenging.

Although many hybridizing or surface-coating methods involving carbonaceous materials or conductive polymers have been used to extrinsically boost the electrical conductivity and minimize the structural degradation of TMO-based electrodes, some accompanying problems need to be solved, including a multistep and complicated process, uneven distribution of each component in the resultant compo-

Received: March 1, 2019
Accepted: April 12, 2019
Published: April 12, 2019

DOI: 10.1021/acsami.9b03830
ACS Appl. Mater. Interfaces 2019, 11, 16647−16655

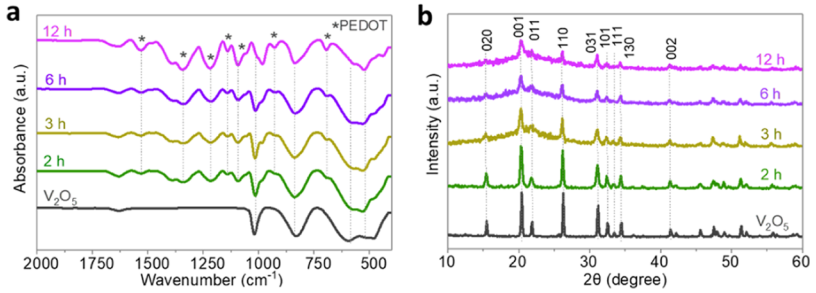

Figure 1. (a) FTIR spectra and (b) XRD patterns of Vö-V_2O_5/PEDOT under 2, 3, 6, 12 h, and pristine V_2O_5.

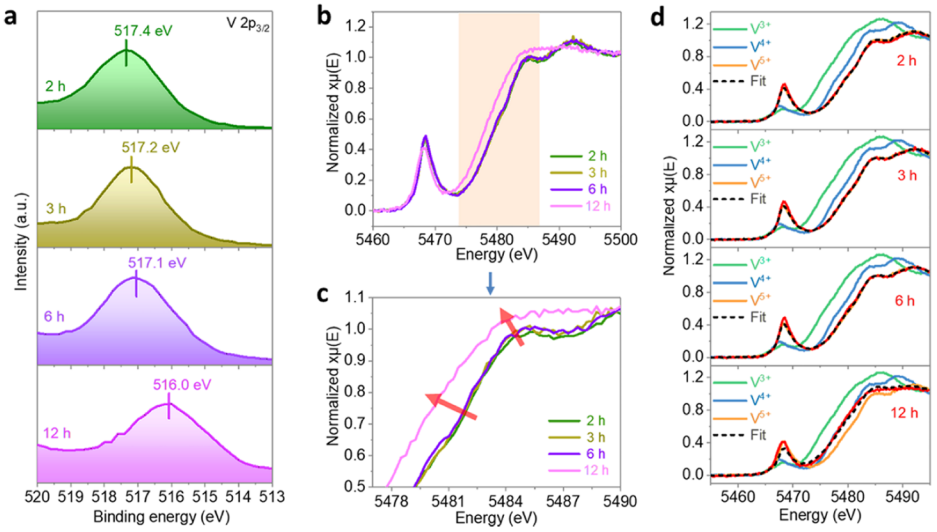

Figure 2. (a) XPS V $2p_{3/2}$ spectra of duration-dependent Vö-V_2O_5/PEDOT with a peak shift to lower binding energy. (b) Normalized V K-edge X-ray absorption near edge structure (XANES) spectra of duration-dependent Vö-V_2O_5/PEDOT. (c) Zoom patterns of the shallow area in (b). An edge shift to lower energies suggests more Vö are created with longer time. (d) The references and model resulting from linear combination fitting of XANES spectra of Vö-V_2O_5/PEDOT. Experimental information for samples is marked with red lines. An obvious shift occurs to the sample in 12 h.

sites.[23,24] Generating defects in TMOs has been investigated as another effective route to intrinsically address the above-mentioned problems by triggering changes in the electronic structure.[25] Specifically, oxygen vacancies (Vö) can provide more void sites for redox reactions and boost charge transfer/transport, enhancing the performance of TMO electrode materials in energy storage.[26,27] Among TMOs, V_2O_5 is reported as an attractive electrode material for supercapacitors due to its high theoretical specific capacitance (2025 F g^{-1}), excellent compatibility with neutral electrolytes, natural abundance, and low cost.[28−30] Furthermore, incorporating Vö into V_2O_5 can improve the electron and ion transport characteristics in the lattice of V_2O_5, enhancing Li^+ ion intercalation.[31] However, it is still unclear how the electrochemical properties of V_2O_5 will be affected, either detrimentally or beneficially, by low- and high-density Vö. Therefore, systematically in-depth explorations of Vö, including the tunable synthesis, formation mechanism, and their effects on energy storage are necessary.

Our previous work introduced and demonstrated the concept of gradient Vö in V_2O_5/PEDOT, effectively impacting the electrochemical properties and the resulting supercapacitor performances.[32] This work tailored the concentration of oxygen vacancies in the surface region of V_2O_5 nanofibers (V_2O_5-NF) by tuning the one-pot in situ oxidative polymerization of PEDOT and systematically studied the fundamental relationships among the processing conditions, concentrations of oxygen vacancies, the thickness of PEDOT coatings, the electrochemical properties, and supercapacitive charge storage performance. The concentration of Vö is facilely tailored in the surface layer of V_2O_5-NF by controlling the one-pot oxidative polymerization of PEDOT, including polymerization duration and polymerization process repetition. Applied in supercapacitors, the redox conversion is synergistically catalyzed with propelled electron/Na^+ transport in the vacancy-enriched layer. The electrochemical performance of the Vö-V_2O_5/PEDOT-based electrode manifests improvement, followed by detriment as more Vö are induced by a thicker PEDOT layer. A durable cycling performance is also obtained after 10 000 cycles. The reasons for the electrochemical performance are explored.

RESULTS AND DISCUSSION

Oxygen vacancies (Vö) form in the surface region of V_2O_5-NF via the oxidative polymerization of PEDOT in a vacuum (Experimental Section in the Supporting Information). Vö in Vö-V_2O_5/PEDOT are firstly tuned by polymerization duration (2−12 h). The sample color changes from yellow to dark blue, indicating an increasing PEDOT content and low valence vanadium ions, as shown in Figure S1a. In Fourier transform infrared (FTIR) spectra (Figure 1a), besides the characteristic bands of V_2O_5 from 1016 to 416 cm^{-1}, the additional peaks

DOI: 10.1021/acsami.9b03830
ACS Appl. Mater. Interfaces 2019, 11, 16647−16655

(marked with *) located at 1522 (aromatic C=C stretching vibrations) and 1397 cm^{-1} (C−C stretching), peaks at 1207, 1143, and 1090 cm^{-1} (C−O−C bond stretching), and peaks at 934, 833, and 692 cm^{-1} (C−S bond stretching vibrations) confirm the existence of PEDOT in Vö-V_2O_5/PEDOT.[33] Progressively strong peaks belonging to PEDOT suggests a larger PEDOT content. X-ray diffraction (XRD) patterns (Figure 1b) present all Vö-V_2O_5/PEDOT samples with a highly pure phase of V_2O_5, in which peaks can be well indexed to the standard PDF card No. 89-0612. This suggests that the main phase of V_2O_5-NF is unchanged by the polymerization of PEDOT. In Figure S1b, the full width at half maximum of the (001) peak increases as polymerization duration prolongs, indicating a lower degree of crystallinity, which is further confirmed by the decreasing peak intensity of Vö-V_2O_5/PEDOT. The loss in crystallinity are possibly attributed to the Vö and PEDOT. Thermogravimetric-differential scanning calorimetry (TG-DSC) analysis (Figure S2) shows a linear increase in the mass content of PEDOT from 8 to 14, 27, and 47% as the polymerization process lasts from 2 to 12 h.[34]

Figure 2a shows the surface oxidation state of vanadium in Vö-V_2O_5/PEDOT, characterized by X-ray photoelectron spectroscopy (XPS). The V $2p_{3/2}$ peak shifts to low binding energy regions as duration extends, indicating a lower valence state of vanadium cations. The V $2p_{3/2}$ peak is decomposed into three peaks as V^{5+}, V^{4+}, and V^{3+} in Figure S3, and the peak area percentage represents the concentration of each oxidation state of vanadium. The concentration of V^{5+} is 90.3% in V_2O_5-NF, and it reduces to 82.0, 69.7, 52.0, and 5.2% in Vö-V_2O_5/PEDOT with the duration being increased to 2, 3, 6, and 12 h, respectively, accompanied by the average valence of vanadium dropping to 4.8, 4.6, 4.4, and 3.6, respectively. The partial reduction of V^{5+} to V^{4+} and V^{3+} species in Vö-V_2O_5/PEDOT should be caused by Vö in V_2O_5 because the reaction occurs without oxygen (vacuum) and only the V_2O_5 phase is detected in all samples by XRD measurements.[32,35] Moreover, with the fixed probing depth (several nanometers) of XPS technology, the detected depth of vanadium reduces when the PEDOT layer gets thicker. Thus, large percentages of Vö from the XPS analysis are due to surface-layer characterization of Vö-V_2O_5/PEDOT nanocables.

With the above local evidence of Vö in Vö-V_2O_5/PEDOT from XPS, X-ray absorption near edge structure (XANES) measurements were adopted to examine the overall Vö in as-prepared Vö-V_2O_5/PEDOT. Detailed measurements and subsequent analysis[36] can be found in the Supporting Information. The XANES spectra of Vö-V_2O_5/PEDOT in Figure 2b,c reveal a shift in the V K-edge toward lower photon energies for longer reaction times, suggesting a reduction of V^{5+} as a result of more Vö created in the heavily coated Vö-V_2O_5/PEDOT. This is consistent with the empirical standards (commercial V_2O_3, VO_2, and V_2O_5), which exhibit several characteristic spectral features, including well-separated edge positions that move to lower energies upon reduction (Figure 2d), as expected.[37] The slight difference in the shape of the pre-edge feature and the precise edge position is a general behavior observed in nanoscale compounds.[38] The reduced vanadium sites are described by V^{4+} and V^{3+}.[39−42] The XANES curves of V_2O_5-NF and V^{5+} agree well in Figure S5c. A little shift in the edge position was observed in samples in 2 and 3 h in Figure 2d. However, an edge shift is progressively observed starting in the sample in 6 h, and it becomes obvious in the sample in 12 h. The spectral fitting results show that the overall concentration of V^{5+} in Vö-V_2O_5/PEDOT decreases from 100 to 99.4, 98.7, and 68.6%, and the concentration of Vö (V^{3+} and V^{4+}) increases accordingly from 0 to 0.6, 1.3, and 31.4%. Consistent with XRD and XPS analyses, more Vö are introduced with more PEDOT. With V^{5+} in the core and Vö near the surface region, it is reasonable that a smaller value of Vö is delivered by XANES measurements than XPS results, because XANES focuses on the bulk of a sample, while XPS examines the differences in the surface layer. This is the first example of the combination of XPS with modern laboratory-based XAFS,[43−45] providing an interesting new paradigm for high-access discrimination of surface and bulk oxygen defect behavior in nanophase systems.

Scanning electron microscopy (SEM) images (Figure 3a−d) present a uniform PEDOT wrapping on the surface of V_2O_5-NF, and the thickness of coating can be observed by a transmission electron microscope (TEM). In Figure 3e−h, a dark V_2O_5-NF core wrapped by a uniform and light PEDOT shell is observed in all Vö-V_2O_5/PEDOT samples. As the polymerization duration is extended to 12 h, the PEDOT shell becomes thicker from ∼1.8 to ∼3.2, ∼5.0, and ∼12.2 nm. Therefore, the thickness of the PEDOT shell is duration-dependent, which is consistent with the FTIR and TG-DSC results. Figure 3i shows the representative high-angle annular dark-field scanning transmission electron microscopy (HADDF-STEM) image of Vö-V_2O_5/PEDOT in 12 h. The corresponding energy dispersive X-ray spectrometry (EDS) elemental mapping analysis (Figure 3i) and line scan profile (Figure 3j) further evidence the uniform distribution of PEDOT, where S is uniformly distributed on the surface, and V and O are throughout the nanowire. Combining all of the results together, tunable Vö are realized in the near surface region of Vö-V_2O_5/PEDOT by controlling the PEDOT thickness, as schematically illustrated in Figure 3k.

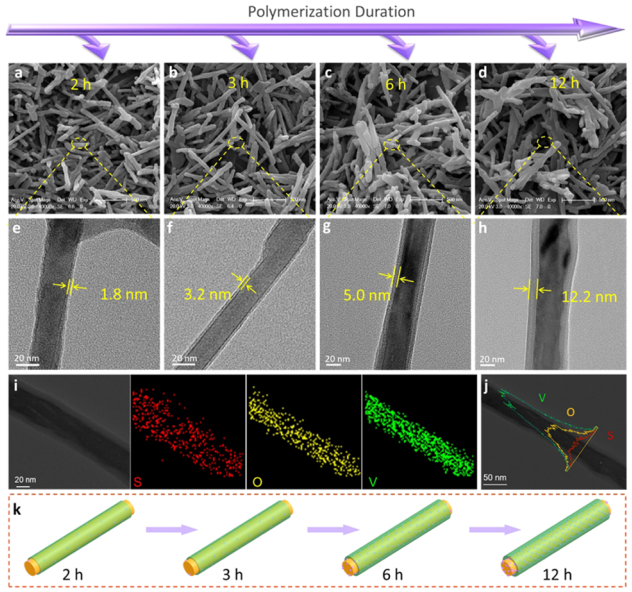

Figure 3. SEM images (a−d) and TEM images (e−h) of duration-dependent Vö-V_2O_5/PEDOT nanocables with a PEDOT coating of ∼1.8, ∼3.2, ∼5.0, and ∼12.2 nm, respectively. (i) HADDF-STEM-EDS elemental maps and (j) line scanning profile of Vö-V_2O_5/PEDOT nanocables in 12 h. (k) Schematic illustration of the concentration of Vö induced in Vö-V_2O_5/PEDOT by thicker PEDOT.

DOI: 10.1021/acsami.9b03830
ACS Appl. Mater. Interfaces 2019, 11, 16647−16655

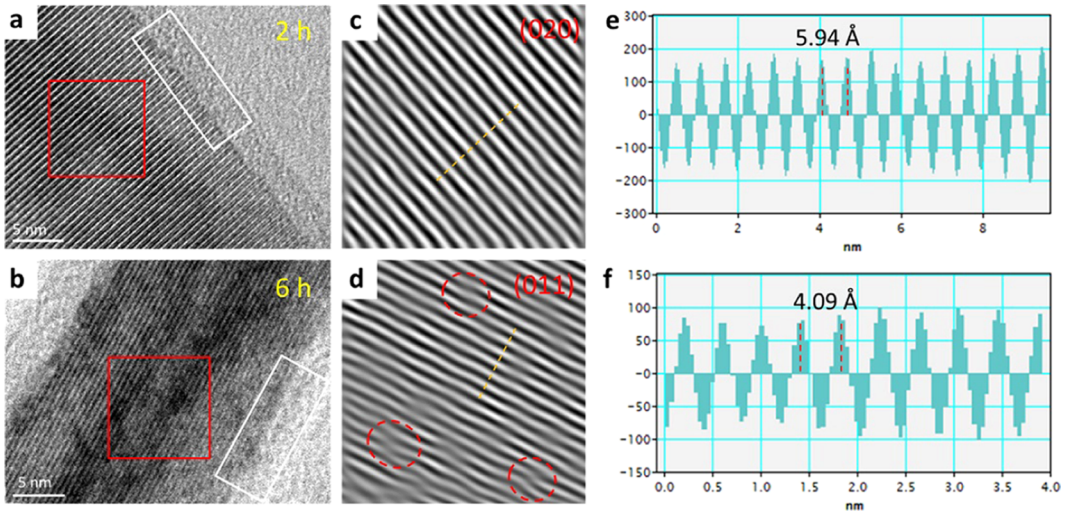

Figure 4. (a, b) HRTEM images of Vö-V_2O_5/PEDOT at 2 and 6 h, respectively. (c, d) IFFT patterns of selected areas (red) in (a) and (b). The red circles show Vö-caused dislocations. (e, f) Linear profiles obtained from the yellow lines in the corresponding IFFT images, showing lattice finger values of 5.94 and 4.09 Å, respectively.

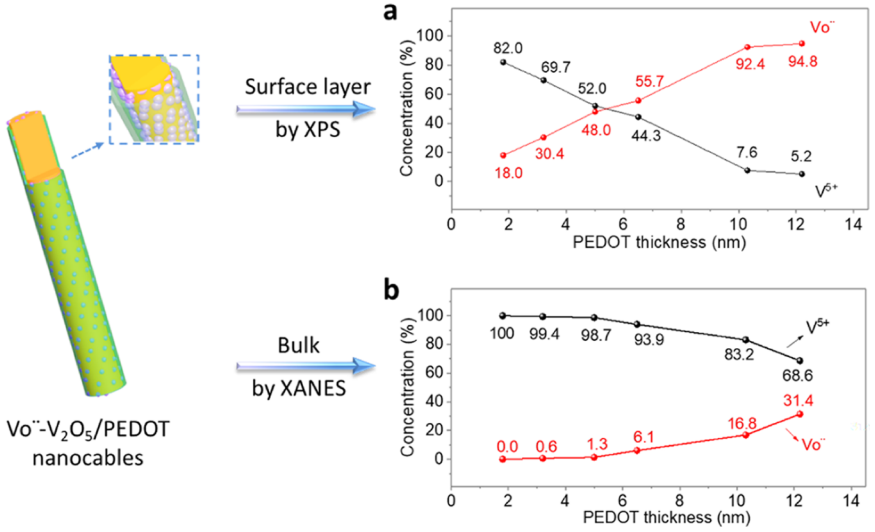

Figure 5. Concentration of Vö in various Vö-V_2O_5/PEDOT nanocables from (a) XPS results for surface-layer characterization and (b) XANES results for overall characterization.

From the above results, it is found that samples in 2 and 6 h exhibit obvious differences in the concentration of Vö. Thus, electron-structural characterization and analysis will be focused on both of them. Compared with high-resolution transmission electron microscopy (HRTEM) image of Vö-V_2O_5/PEDOT in 2 h (Figure 4a), the sample in 6 h shows additional mottled points between lattice fringes and an ambiguous boundary (marked with white) in Figure 4b. In Figure 4c,e, inverse fast Fourier transform (IFFT) technique-enhanced HRTEM of sample in 2 h demonstrates perfect lattice fringes with a lattice parameter of $d_{2\ h}$ = 5.94 Å, larger than the corresponding standard parameter (5.76 Å) of the (020) facet of V_2O_5 (No. 89-0612). This can be explained that the V_2O_5 crystal lattice is expanded when Vö donate electrons to the empty 3d-orbitals of V_2O_5 and increase the ionic radius of vanadium ion (V^{4+} and V^{3+}). With a larger concentration of Vö, Vö clusters will be formed to alleviate internal strain and retain stable lattices.[46] As a result, dislocations (in red circles) are clearly observed in the IFFT image of the sample in 6 h, accompanied by an unchanged lattice finger of $d_{6\ h}$ = 4.09 Å, which belongs to the (011) panel of V_2O_5 (Figure 4d,f). These discrepant dislocations further confirm the tunable concentrations of Vö in Vö-V_2O_5/PEDOT, consistent with XPS and XANES analysis. As more Vö are created in Vö-V_2O_5/PEDOT, more valence electrons can be donated and more voids for receiving electrons, and efficient diffusion paths for ions, which will facilitate charge transfer kinetics and energy storage.[47,48]

The concentration of Vö in Vö-V_2O_5/PEDOT is not only related to polymerization duration, but also can be tailored by polymerization process (3 h) repetition. More Vö are induced by a thicker PEDOT layer in the repetition process. Characterization and analysis are shown in the Supporting Information and Figures S4−S7. For clarity, the local and overall concentration of Vö of all Vö-V_2O_5/PEDOT samples from XPS and XANES measurements are respectively summarized in Figure 5. As the thickness of the PEDOT layer changes from ∼1.8 to ∼3.2, ∼5.0, ∼6.5, ∼10.3, and ∼12.2 nm, the associated surface-layer concentration of Vö increases

DOI: 10.1021/acsami.9b03830
ACS Appl. Mater. Interfaces 2019, 11, 16647−16655

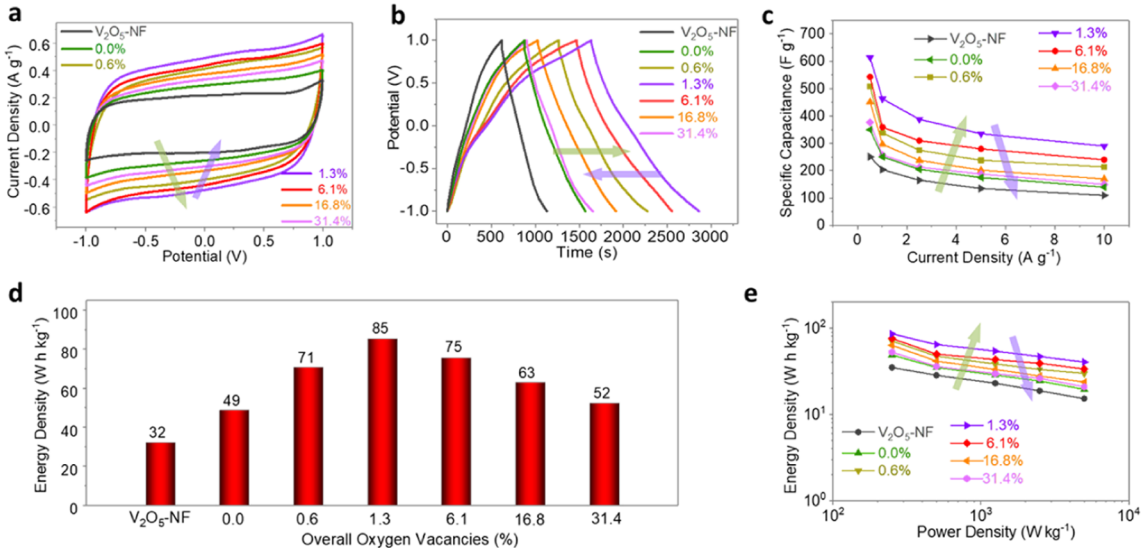

Figure 6. (a) CV curves at 5 mV s^{-1} and (b) GCD curves at 0.5 A g^{-1} of V_2O_5-NF and all Vö-V_2O_5/PEDOT samples. (c) Specific capacitances of all samples at different current densities. (d) The energy density of Vö-V_2O_5/PEDOT as a function of Vö. The power density is 250 W kg^{-1}. The sample with 1.3% overall concentration of Vö manifests the highest energy density. (e) Ragone plots of different Vö-V_2O_5/PEDOT and V_2O_5-NF electrodes.

from 18.0 to 30.4, 48.0, 55.7, 92.4, and 94.8% (Figure 5a), and the overall value raises from 0.0 to 0.6, 1.3, 6.1, 16.8, and 31.4% (Figure 5b).

With a tailored concentration of Vö in Vö-V_2O_5/PEDOT, their effects on the electrochemical performance of Vö-V_2O_5/PEDOT-based supercapacitors were studied by performing cyclic voltammetry (CV) and galvanostatic charge/discharge (GCD) in 1 M Na_2SO_4 aqueous solution. Each sample is noted by its overall concentration of Vö from XANES measurements. As shown in Figures 6a and S8a–g, all Vö-V_2O_5/PEDOT electrodes exhibit surpercapacitive behaviors with quasi-rectangular CV loops (scan rate ranging from 5 to 100 mV s^{-1}). Compared with V_2O_5-NF, larger voltammogram areas of all Vö-V_2O_5/PEDOT samples indicate an improvement in charge storage capability. All of the GCD curves appear with tilted triangle shapes at different current densities from 0.5 to 10.0 A g^{-1} (Figures 6b and S9a–g). The specific capacitance was calculated with the discharging curves at 0.5 A g^{-1} in Figure 6b. Interestingly, the highest value is achieved at 614 F g^{-1} when the overall concentration of Vö is at 1.3% (~5.0 nm PEDOT layer); the specific capacitance decreases subsequently to 377 F g^{-1} with more Vö, but still higher than V_2O_5-NF (231 F g^{-1}). The same occurs to specific capacitances under various current densities in Figure 6c. This phenomenon can be ascribed to Vö and PEDOT, which will be explored in the next paragraph. The specific capacitance is higher than that of other V_2O_5-based supercapacitors, such as V_2O_5 networks (316 F g^{-1}),[49] V_2O_5/PEDOT/MnO_2 (266 F g^{-1}),[50] core–shell V_2O_5@PPy (308 F g^{-1}),[13] and V_2O_5/carbon composites (295 F g^{-1}).[51] Accordingly, Vö-V_2O_5/PEDOT nanocables with 1.3% Vö in bulk deliver a high energy density up to 85 W h kg^{-1} with a power density ranging from 250 to 2500 W kg^{-1}, as shown in Figure 6d,e. These results suggest that the capacitance and energy density of Vö-V_2O_5/PEDOT are effectively optimized by Vö.

Electrochemical impedance spectra (EIS) and the equivalent circuit model were used to reveal kinetic reasons for the electrochemical performance of Vö-V_2O_5/PEDOT electrodes. In an EIS curve, a semicircle and a sloping line are related to charge transfer resistance (R_{ct}) at the electrode/electrolyte interface and ion diffusion in a solid electrode, respectively; the ohmic resistance value (R_s) corresponds to the cell's internal resistance. As shown in Figures 7b and S10, the decreasing value of R_{ct} (from 6.17 to 1.95, 8.47 Ω for V_2O_5-NF) suggests that the charge transfer kinetics is dramatically enhanced with a

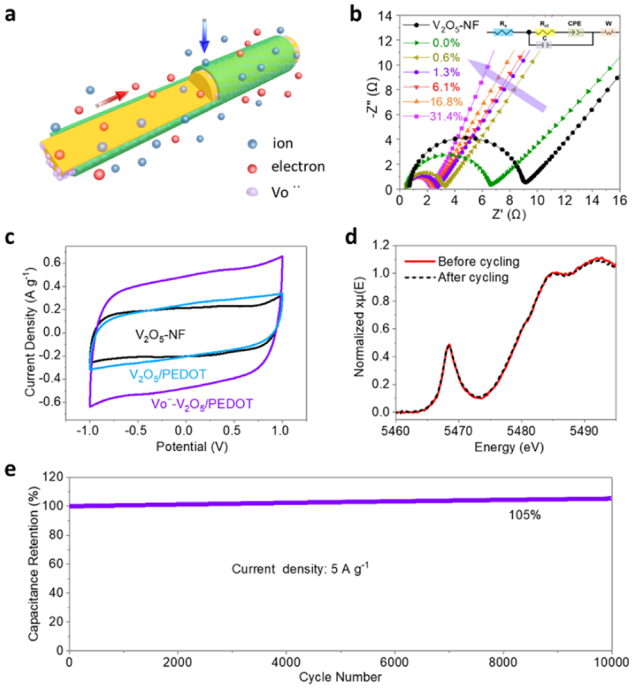

Figure 7. (a) Schematic illustration of charge transfer in Vö-V_2O_5/PEDOT nanocables. The kinetics is enhanced by both Vö and PEDOT. (b) EIS spectra of all samples with the equivalent circuit model being inseted. (c) CV curves of Vö-V_2O_5/PEDOT with 1.3% Vö, mixed V_2O_5/PEDOT, and V_2O_5-NF. (d) XANES spectra of Vö-V_2O_5/PEDOT with 1.3% Vö before and after cycling. (e) Cycling performance of Vö-V_2O_5/PEDOT with 1.3% Vö. No visible degradation is observed.

DOI: 10.1021/acsami.9b03830
ACS Appl. Mater. Interfaces 2019, 11, 16647–16655

larger concentration of Vö. Slight changes in R_s (from 0.48 to 0.44 Ω) suggest few effects from this cell; the Vö-V_2O_5/PEDOT electrode delivers a gradually steeper slope with more Vö and PEDOT, suggesting faster Na^+ ion diffusion.[52,53] The significantly improved charge transfer and Na^+ ion diffusion promoted redox reactions and enhanced capacitive capability of Vö-V_2O_5/PEDOT due to the synergy between Vö and the PEDOT layer, as shown in Figure 7a. Specifically, Vö in the crystal lattice provide more void spaces and channels for faster and easier ion diffusion/storage, achieving a higher specific capacitance,[54] consistent with IFFT image analysis. In addition, the PEDOT shell shortens the charge transfer/transport distance and promotes charge transport with its excellent conductive properties, leading to much enhanced kinetics for redox reactions.[50] This synergistic effect was further proved by mechanically grinding V_2O_5-NF and commercial PEDOT with a mass ratio from the TG result of Vö-V_2O_5/PEDOT with 1.3% Vö. Consistent with the CV loops (5 mV s^{-1}) in Figure 7c, the resultant V_2O_5/PEDOT (without Vö) exhibits a much smaller specific capacitance (285 F g^{-1}) than Vö-V_2O_5/PEDOT (614 F g^{-1}), but larger than V_2O_5-NF (231 F g^{-1}) at 0.5 A g^{-1}. Detailed information can be found in Figure S11. Considering the fact that redox reactions between V^{5+} and V^{4+}, V^{3+} contribute to the high capacitance of V_2O_5-based electrodes,[52] the sharp decrease in V^{5+} (from 98.7 to 68.6%) for excessive Vö will compromise Faradic reactions and finally lead to reduced energy density. A thicker PEDOT shell may also introduce charge transport resistance, lowering the capacitance.[55] However, the capacitance contribution of PEDOT might be small and negligible. First of all, the capacitance of Vö-V_2O_5/PEDOT nanocables mainly derives from redox reactions in V_2O_5 and the double-layer contribution would be very small. Secondly, there is no experimental evidence showing possible redox reactions of PEDOT in the current testing conditions as shown in CV curves. Thirdly, V_2O_5/PEDOT (only with PEDOT physically admixed) did not show an appreciable increase in capacitance. Therefore, the storage capacitance of Vö-V_2O_5/PEDOT is optimized when the overall concentration of Vö is 1.3%.

Vö-V_2O_5/PEDOT electrodes with 1.3% Vö manifest an excellent cycling performance with 105% capacitance retention after 10 000 charge/discharge cycles at 5 A g^{-1}, shown in Figure 7e. The stability originates from the PEDOT shell, which prevents V_2O_5 from collapsing,[24] and Vö, which can alleviate the electrochemically induced strain between layers in the charge/discharge process.[46] Since the concentration of Vö is unchanged after cycling, confirmed by XANES in Figure 7d, increased capacitance should be caused by the homogenous distribution of Vö driven by the electric field applied in the cycling process, which is further evidenced by density functional theory (DFT) in the following paragraph. When the applied electric field drives electrolyte ions to the electrode for redox reactions, the Vö-V_2O_5/PEDOT electrode surface may be further wet and electroactivated, similar to that reported in the literature,[56,57] which is another possible reason for the increased capacitance. In addition, this cyclability is superior to other vanadium oxide-based supercapacitors and PEDOT-based supercapacitors, such as V_2O_5/PEDOT/MnO_2 nanosheets (93.5% capacitance retention after 3000 cycles),[50] graphene/V_2O_5 (93.7% capacitance retention after 10 000 cycles),[58] PEDOT paper (93% capacitance retention after 15 000 cycles),[59] and MnO_2@PEDOT@MnO_2 (91.3% retention after 5000 cycles).[55]

Density functional theory (DFT) was applied to investigate migration of Vö in Vö-V_2O_5/PEDOT, and detailed calculations are shown in the Supporting Information. Two kinds of Vö are examined: one kind of Vö locates outside of the top V_2O_5 layer, (Figure 8a); the other kind of Vö is inside of the top V_2O_5 layer (Figure 8b). From the DFT calculations, the Gibbs free energy of the former (G_{out}) is estimated at −306.58 eV and the value of the latter (G_{in}) is −306.88 eV, which suggests that it is energetically possible for Vö to form in the inner layers of V_2O_5. Moreover, the top-layer Vö induces the formation of V^{4+}−O−V^{4+} below. When the Vö moves into the inner layer of V_2O_5, V^{4+}−O−V^{4+} also migrates into the inner layers. Since the formation ratio of defects normally depends on the Gibbs Free energy (G), as follows

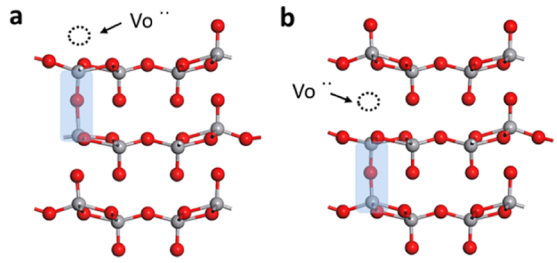

Figure 8. DFT calculations for the migration of Vö in V_2O_5. (a) Vö locates outside of the top V_2O_5 layer with a Gibbs free energy of −306.58 eV (b) Vö is inside of the top V_2O_5 layer with a Gibbs free energy of −306.88 eV, accompanied by the V^{4+}−O−V^{4+} (blue shade) moved inward.

$$n/N = e^{-\Delta G/kBT}$$

where n is the number of defects on the surface, N is the total number of atoms, ΔG is the formation energy of two balance states, k_B is the Boltzmann constant, and T is the temperature. Here, ΔG is the difference between Gibbs Free energy G_{out} and G_{in}. Therefore, approximately 9.75×10^{-6} of total atoms of Vö will migrate into the inner layers of V_2O_5 at room temperature (300 K). Consistent with XANES analysis, this calculation result further confirms the migration of Vö. This calculation is applicable for other V_2O_5 samples with Vö distributed at the surface and provides reference for other Vö contained transmission metal oxides.

CONCLUSIONS

Oxygen vacancies (Vö) have been created in the near surface region of V_2O_5/PEDOT nanocables (Vö-V_2O_5/PEDOT) and applied as electrode materials for high-energy and durable supercapacitors. XPS and XANES measurements show that the concentration of Vö in Vö-V_2O_5/PEDOT increases as the PEDOT shell becomes thicker from ∼1.8 to ∼12.2 nm. Vö-V_2O_5/PEDOT nanocables with an overall concentration of Vö of 1.3% deliver a high energy density (85 W h kg^{-1} with a power density at 250 W kg^{-1}) and a prolonged cycling life (105% capacitance retention after 10 000 cycles at 5 A g^{-1}), due to the synergy between Vö and PEDOT in enhancing the charge transfer and ion diffusion kinetics and cycling stability. This work not only explores the effects of tunable Vö on the electrochemical performance of V_2O_5-based supercapacitors but also provides an in-depth understanding of Vö for other transition metal oxides (like Fe_2O_3, MoO_3, etc.) in energy storage.

DOI: 10.1021/acsami.9b03830
ACS Appl. Mater. Interfaces 2019, 11, 16647−16655

■ ASSOCIATED CONTENT

Supporting Information

The Supporting Information is available free of charge on the ACS Publications website at DOI: 10.1021/acsami.9b03830.

Experimental information, TG-DSC curves, and XPS analysis of duration-dependent Vö-V_2O_5/PEDOT; characterization of poly.-dependent Vö-V_2O_5/PEDOT; electrochemical performance of all Vö-V_2O_5/PEDOT samples, V_2O_5/PEDOT, and V_2O_5-NF (PDF)

■ AUTHOR INFORMATION

Corresponding Authors

*E-mail: gao@tongji.edu.cn (G.G.).
*E-mail: wugm@tongji.edu.cn (G.W.).
*E-mail: gzcao@u.washington.edu (G.C.).

ORCID

Gerald Seidler: 0000-0001-6738-7930
Guozhong Cao: 0000-0001-6539-0490

Notes

The authors declare no competing financial interest.

■ ACKNOWLEDGMENTS

The authors W.B., J.W., G.G., and G.W. acknowledge the financial support of the National Natural Science Foundation of China (Grants U1503292, 51472182, 51872204), the Fundamental Research Funds for the Central Universities, and the National Key Research and Development Program of China (Grant 2017YFA0204600). W.B. acknowledges the support from the China Scholarship Council (CSC) for studying at the University of Washington. The authors W.B., and G.C. also acknowledge the support from the National Science Foundation (1803256). The authors W.B., M.A., M.A., and G.C. extend their appreciation to the support from the International Scientific Partnership Program (ISPP-139) at King Saud University. E.J. was supported by a subcontract from the National Institute of Standards and Technology. Opinions, recommendations, findings, and conclusions presented in this manuscript and associated materials do not necessarily reflect the views or policies of NIST or the United States Government. Part of this work was conducted at the Molecular Analysis Facility, a National Nanotechnology Coordinated Infrastructure site at the University of Washington, which is supported in part by the National Science Foundation (Grant NNCI-1542101), the University of Washington, the Molecular Engineering & Sciences Institute, and the Clean Energy Institute.

■ REFERENCES

(1) Cui, P.; Wei, D.; Ji, J.; Huang, H.; Jia, E.; Dou, S.; Wang, T.; Wang, W.; Li, M. Planar p−n Homojunction Perovskite Solar Cells with Efficiency Exceeding 21.3%. *Nat. Energy* **2019**, 150.

(2) Yang, Y.; Zhao, X.; Wang, H.-E.; Li, M.; Hao, C.; Ji, M.; Ren, S.; Cao, G. Phosphorized Sno_2/Graphene Heterostructures for Highly Reversible Lithium-Ion Storage with Enhanced Pseudocapacitance. *J. Mater. Chem. A* **2018**, *6*, 3479−3487.

(3) Zhao, X.; Cai, W.; Yang, Y.; Song, X.; Neale, Z.; Wang, H.-E.; Sui, J.; Cao, G. MoSe2 Nanosheets Perpendicularly Grown on Graphene with Mo−C Bonding For Sodium-Ion Capacitors. *Nano Energy* **2018**, *47*, 224−234.

(4) Zhao, X.; Wang, H.-E.; Massé, R. C.; Cao, J.; Sui, J.; Li, J.; Cai, W.; Cao, G. Design of Coherent Anode Materials with 0d Ni3s2 Nanoparticles Self-Assembled on 3d Interconnected Carbon Networks for Fast and Reversible Sodium Storage. *J. Mater. Chem. A* **2017**, *5*, 7394−7402.

(5) Sheberla, D.; Bachman, J. C.; Elias, J. S.; Sun, C. J.; Shao-Horn, Y.; Dinca, M. Conductive MOF Electrodes for Stable Supercapacitors with High Areal Capacitance. *Nat. Mater.* **2017**, *16*, 220−224.

(6) Mai, L. Q.; Minhas-Khan, A.; Tian, X.; Hercule, K. M.; Zhao, Y. L.; Lin, X.; Xu, X. Synergistic Interaction between Redox-Active Electrolyte and Binder-Free Functionalized Carbon for Ultrahigh Supercapacitor Performance. *Nat. Commun.* **2013**, *4*, No. 2923.

(7) Cao, F.; Zhao, M.; Yu, Y.; Chen, B.; Huang, Y.; Yang, J.; Cao, X.; Lu, Q.; Zhang, X.; Zhang, Z.; Tan, C.; Zhang, H. Synthesis of Two-Dimensional CoS1.097/Nitrogen-Doped Carbon Nanocomposites Using Metal-Organic Framework Nanosheets as Precursors for Supercapacitor Application. *J. Am. Chem. Soc.* **2016**, *138*, 6924−6927.

(8) Béguin, F.; Presser, V.; Balducci, A.; Frackowiak, E. Carbons and Electrolytes for Advanced Supercapacitors. *Adv. Mater.* **2014**, *26*, 2219−2251.

(9) Ellis, B. L.; Knauth, P.; Djenizian, T. Three-Dimensional Self-Supported Metal Oxides for Advanced Energy Storage. *Adv. Mater.* **2014**, *26*, 3368−3397.

(10) Stoller, M. D.; Ruoff, R. S. Best Practice Methods for Determining an Electrode Material's Performance for Ultracapacitors. *Energy Environ. Sci.* **2010**, *3*, 1294−1301.

(11) Li, M.; Sun, G.; Yin, P.; Ruan, C.; Ai, K. Controlling the Formation of Rodlike V_2O_5 Nanocrystals on Reduced Graphene Oxide for High-Performance Supercapacitors. *ACS Appl. Mater. Interfaces* **2013**, *5*, 11462−11470.

(12) Chen, L. F.; Lu, Y.; Yu, L.; Lou, X. W. Designed Formation of Hollow Particle-Based Nitrogen-Doped Carbon Nanofibers for High-Performance Supercapacitors. *Energy Environ. Sci.* **2017**, *10*, 1777−1783.

(13) Qu, Q. T.; Zhu, Y. S.; Gao, X. W.; Wu, Y. Core-Shell Structure of Polypyrrole Grown on V_2O_5 Nanoribbon as High Performance Anode Material for Supercapacitors. *Adv. Energy Mater.* **2012**, *2*, 950−955.

(14) Bai, M. H.; Liu, T. Y.; Luan, F.; Li, Y.; Liu, X.-X. Electrodeposition of Vanadium Oxide−Polyaniline Composite Nanowire Electrodes for High Energy Density Supercapacitors. *J. Mater. Chem. A* **2014**, *2*, 10882−10888.

(15) Snook, G. A.; Kao, P.; Best, A. S. Conducting-Polymer-based Supercapacitor Devices and Electrodes. *J. Power Sources* **2011**, *196*, 1−12.

(16) Osterholm, A. M.; Ponder, J. F., Jr.; Kerszulis, J. A.; Reynolds, J. R. Solution Processed PEDOT Analogues in Electrochemical Supercapacitors. *ACS Appl. Mater. Interfaces* **2016**, *8*, 13492−13498.

(17) Jiang, Q.; Kurra, N.; Alhabeb, M.; Gogotsi, Y.; Alshareef, H. N. All Pseudocapacitive MXene-RuO2 Asymmetric Supercapacitors. *Adv. Energy Mater.* **2018**, *8*, 1703043−1703050.

(18) Yang, S.; Liu, Y.; Hao, Y.; Yang, X.; Goddard, W. A., 3rd; Zhang, X. L.; Cao, B. Oxygen-Vacancy Abundant Ultrafine Co3O4/Graphene Composites for High-Rate Supercapacitor Electrodes. *Adv. Sci.* **2018**, *5*, No. 1700659.

(19) Cao, L.; Zhu, J.; Li, Y.; Xiao, P.; Zhang, Y.; Zhang, S.; Yang, S. Ultrathin Single-Crystalline Vanadium Pentoxide Nanoribbon Constructed 3D Networks for Superior Energy Storage. *J. Mater. Chem. A* **2014**, *2*, 13136−13142.

(20) Pan, A.; Wu, H. B.; Yu, L.; Zhu, T.; Lou, X. W. Synthesis of Hierarchical Three-Dimensional Vanadium Oxide Microstructures as High-Capacity Cathode Materials for Lithium-Ion Batteries. *ACS Appl. Mater. Interfaces* **2012**, *4*, 3874−3879.

(21) Simon, P.; Gogotsi, Y. Materials for Electrochemical Capacitors. *Nat. Mater.* **2008**, *7*, 845−854.

(22) Yu, L.; Yu, X. Y.; Lou, X. W. D. The Design and Synthesis of Hollow Micro-/Nanostructures: Present and Future Trends. *Adv. Mater.* **2018**, *30*, No. 1800939.

(23) Wang, Y.; Fu, X.; Zheng, M.; Zhong, W. H.; Cao, G. Strategies for Building Robust Traffic Networks in Advanced Energy Storage Devices: A Focus on Composite Electrodes. *Adv. Mater.* **2019**, *31*, No. 1804204.

DOI: 10.1021/acsami.9b03830
ACS Appl. Mater. Interfaces 2019, 11, 16647−16655

(24) Mai, L.; Dong, F.; Xu, X.; Luo, Y.; An, Q.; Zhao, Y.; Pan, J.; Yang, J. Cucumber-Like V_2O_5/poly(3,4-ethylenedioxythiophene) &MnO_2 Nanowires with Enhanced Electrochemical Cyclability. *Nano Lett.* **2013**, *13*, 740−745.
(25) Wang, Y.; Xiao, X.; Li, Q.; Pang, H. Synthesis and Progress of New Oxygen-Vacant Electrode Materials for High-Energy Rechargeable Battery Applications. *Small* **2018**, *14*, No. 1802193.
(26) Xu, Y.; Zhou, M.; Zhang, C.; Wang, C.; Liang, L.; Fang, Y.; Wu, M.; Cheng, L.; Lei, Y. Oxygen Vacancies: Effective Strategy to Boost Sodium Storage of Amorphous Electrode Materials. *Nano Energy* **2017**, *38*, 304−312.
(27) Kim, H. S.; Cook, J. B.; Lin, H.; Ko, J. S.; Tolbert, S. H.; Ozolins, V.; Dunn, B. Oxygen Vacancies Enhance Pseudocapacitive Charge Storage Properties of MoO_{3-x}. *Nat. Mater.* **2017**, *16*, 454−460.
(28) Zhi, M.; Xiang, C. C.; Li, J. T.; Li, M.; Wu, N. Q. Nanostructured Carbon-Metal Oxide Composite Electrodes for Supercapacitors: A Review. *Nanoscale* **2013**, *5*, 72−88.
(29) Wang, Y.; Nie, Z.; Pan, A.; Zhang, Y.; Kong, X.; Zhu, T.; Liang, S.; Cao, G. Self-templating synthesis of double-wall shelled vanadium oxide hollow microspheres for high-performance lithium ion batteries. *J. Mater. Chem. A* **2018**, *6*, 6792−6799.
(30) Perera, S. D.; Patel, B.; Bonso, J.; Grunewald, M.; Ferraris, J. P.; Balkus, K. J., Jr. Vanadium Oxide Nanotube Spherical Clusters Prepared on Carbon Fabrics for Energy Storage Applications. *ACS Appl. Mater. Interfaces* **2011**, *3*, 4512−4517.
(31) Scanlon, D. O.; Walsh, A.; Morgan, B. J.; Watson, G. W. An ab initio Study of Reduction of V_2O_5 through the Formation of Oxygen Vacancies and Li Intercalation. *J. Phys. Chem. C* **2008**, *112*, 9903−9911.
(32) Bi, W.; Wu, Y.; Liu, C.; Wang, J.; Du, Y.; Gao, G.; Wu, G.; Cao, G. Gradient Oxygen Vacancies in V_2O_5/PEDOT Nanocables for High-Performance Supercapacitors. *ACS Appl. Energy Mater.* **2019**, *2*, 668−677.
(33) Jiang, C.; Chen, G.; Wang, X. High-Conversion Synthesis of Poly(3,4-Ethylenedioxythiophene) by Chemical Oxidative Polymerization. *Synth. Met.* **2012**, *162*, 1968−1971.
(34) Murugan, A. V.; Kale, B. B.; Kwon, C.-W.; Campet, G.; Vijayamohanan, K. Synthesis and Characterization of A New Organo−Inorganic Poly(3,4-Ethylene Dioxythiophene) Pedot/V_2O_5 Nanocomposite by Intercalation. *J. Mater. Chem.* **2001**, *11*, 2470−2475.
(35) Deng, X.; Wei, Z.; Cui, C.; Liu, Q.; Wang, C.; Ma, J. Oxygen-deficient anatase TiO2@C nanospindles with pseudocapacitive contribution for enhancing lithium storage. *J. Mater. Chem. A* **2018**, *6*, 4013−4022.
(36) Ravel, B.; Newville, M. ATHENA, ARTEMIS, HEPHAESTUS: Data Analysis for X-Ray Absorption Spectroscopy Using IFEFFIT. *J. Synchrotron Radiat.* **2005**, *12*, 537−541.
(37) Bunker, G. *Introduction to XAFS: A Practical Guide to X-Ray Absorption Fine Structure Spectroscopy*; Cambridge University Press, 2010.
(38) Gaur, A.; Shrivastava, B. D. Speciation using X-ray absorption fine structure (XAFS). *Rev. J. Chem.* **2015**, *5*, 361−398.
(39) Teodorescu, C. M.; Socol, G.; Negrila, C.; Luca, D.; Macovei, D. Nanostructured Thin Layers of Vanadium Oxides Doped with Cobalt, Prepared by Pulsed Laser Ablation: Chemistry, Local Atomic Structure, Morphology and Magnetism. *J. Exp. Nanosci.* **2010**, *5*, 509−526.
(40) Powell, M. J.; Godfrey, I. J.; Quesada-Cabrera, R.; Malarde, D.; Teixeira, D.; Emerich, H.; Palgrave, R. G.; Carmalt, C. J.; Parkin, I. P.; Sankar, G. Qualitative XANES and XPS Analysis of Substrate Effects in VO2 Thin Films: A Route to Improving Chemical Vapor Deposition Synthetic Methods? *J. Phys. Chem. C* **2017**, *121*, 20345−20352.
(41) Stewart, S. J.; Fernandez-Garcia, M.; Belver, C.; Mun, B. S.; Requejo, F. G. Influence of N-doping on the Structure and Electronic Properties of Titania Nanoparticle Photocatalysts. *J. Phys. Chem. B* **2006**, *110*, 16482−16486.
(42) Wu, Z. Y.; Zhang, J.; Ibrahim, K.; Xian, D. C.; Li, G.; Tao, Y.; Hu, T. D.; Bellucci, S.; Marcelli, A.; Zhang, Q. H.; Gao, L.; Chen, Z. Z. Structural Determination of Titanium-Oxide Nanoparticles by X-Ray Absorption Spectroscopy. *Appl. Phys. Lett.* **2002**, *80*, 2973−2975.
(43) Jahrman, E. P.; Holden, W. M.; Ditter, A. S.; Mortensen, D. R.; Seidler, G. T.; Fister, T. T.; Kozimor, S. A.; Piper, L. F. J.; Rana, J.; Hyatt, N. C.; Stennett, M. C. An Improved Laboratory-Based X-Ray Absorption Fine Structure and X-Ray Emission Spectrometer for Analytical Applications in Materials Chemistry Research. *Rev. Sci. Instrum.* **2019**, *90*, No. 024106.
(44) Seidler, G. T.; Mortensen, D. R.; Remesnik, A. J.; Pacold, J. I.; Ball, N. A.; Barry, N.; Styczinski, M.; Hoidn, O. R. A laboratory-based hard x-ray monochromator for high-resolution x-ray emission spectroscopy and x-ray absorption near edge structure measurements. *Rev. Sci. Instrum.* **2014**, *85*, No. 113906.
(45) Seidler, G. T.; Mortensen, D. R.; Ditter, A. S.; Ball, N. A.; Remesnik, A. J. A modern laboratory XAFS cookbook. *J. Phys. Conf. Ser.* **2016**, *712*, No. 012015.
(46) Yan, P.; Zheng, J.; Gu, M.; Xiao, J.; Zhang, J. G.; Wang, C. M. Intragranular Cracking as A Critical Barrier for High-Voltage Usage of Layer-Structured Cathode for Lithium-Ion Batteries. *Nat. Commun.* **2017**, *8*, No. 14101.
(47) Xiong, T.; Yu, Z. G.; Wu, H.; Du, Y.; Xie, Q.; Chen, J.; Zhang, Y.-W.; Pennycook, S. J.; Lee, W. S. V.; Xue, J. Defect Engineering of Oxygen-Deficient Manganese Oxide to Achieve High-Performing Aqueous Zinc Ion Battery. *Adv. Energy Mater.* **2019**, No. 1803815.
(48) Hao, J.; Peng, S.; Li, H.; Dang, S.; Qin, T.; Wen, Y.; Huang, J.; Ma, F.; Gao, D.; Li, F.; Cao, G. A Low Crystallinity Oxygen-Vacancy-Rich Co_3O_4 Cathode for High-Performance Flexible Asymmetric Supercapacitors. *J. Mater. Chem. A* **2018**, *6*, 16094−16100.
(49) Saravanakumar, B.; Purushothaman, K. K.; Muralidharan, G. Interconnected V_2O_5 Nanoporous Network for High-Performance Supercapacitors. *ACS Appl. Mater. Interfaces* **2012**, *4*, 4484−4490.
(50) Guo, C. X.; Yilmaz, G.; Chen, S.; Chen, S.; Lu, X. Hierarchical Nanocomposite Composed of Layered V_2O_5/PEDOT/MnO_2 Nanosheets for High-performance Asymmetric Supercapacitors. *Nano Energy* **2015**, *12*, 76−87.
(51) Wang, B.; Konstantinov, K.; Wexler, D.; Liu, H.; Wang, G. Synthesis of nanosized vanadium pentoxide/carbon composites by spray pyrolysis for electrochemical capacitor application. *Electrochim. Acta* **2009**, *54*, 1420−1425.
(52) Zheng, K.; Zeng, Y.; Liu, S.; Zeng, C.; Tong, Y.; Zheng, Z.; Zhu, T.; Lu, X. Valence and Surface Modulated Vanadium Oxide Nanowires as New High-Energy and Durable Negative Electrode for Flexible Asymmetric Supercapacitors *Energy Storage Mater.* 2019, DOI: 10.1016/j.ensm.2019.02.012.
(53) Jia, R.; Yue, J.; Xia, Q.; Xu, J.; Zhu, X.; Sun, S.; Zhai, T.; Xia, H. Carbon shelled porous SnO2-δ nanosheet arrays as advanced anodes for lithium-ion batteries. *Energy Storage Mater.* **2018**, *13*, 303−311.
(54) Yu, M.; Zeng, Y.; Han, Y.; Cheng, X.; Zhao, W.; Liang, C.; Tong, Y.; Tang, H.; Lu, X. Valence-Optimized Vanadium Oxide Supercapacitor Electrodes Exhibit Ultrahigh Capacitance and Super-Long Cyclic Durability of 100 000 Cycles. *Adv. Funct. Mater.* **2015**, *25*, 3534−3540.
(55) Tang, P.; Han, L.; Zhang, L.; Wang, S.; Feng, W.; Xu, G.; Zhang, L. Controlled Construction of Hierarchical Nanocomposites Consisting of MnO_2 and PEDOT for High-Performance Supercapacitor Applications. *ChemElectroChem* **2015**, *2*, 949−957.
(56) Wu, Y. J.; Gao, G. H.; Yang, H. Y.; Bi, W.; Liang, X.; Zhang, Y.; Zhang, G.; Wu, G. Controlled Synthesis of V_2O_5/MWCNT Core/Shell Hybrid Aerogels through a Mixed Growth and Self-Assembly Methodology for Supercapacitors with High Capacitance and Ultralong Cycle Life. *J. Mater. Chem. A* **2015**, *3*, 15692−15699.
(57) Yan, Y.; Cheng, Q.; Zhu, Z.; Pavlinek, V.; Saha, P.; Li, C. Controlled Synthesis of Hierarchical Polyaniline Nanowires/Ordered Bimodal Mesoporous Carbon Nanocomposites with High Surface Area for Supercapacitor Electrodes. *J. Power Sources* **2013**, *240*, 544−550.

DOI: 10.1021/acsami.9b03830
ACS Appl. Mater. Interfaces 2019, 11, 16647−16655

(58) Boruah, B. D.; Nandi, S.; Misra, A. Layered Assembly of Reduced Graphene Oxide and Vanadium Oxide Heterostructure Supercapacitor Electrodes with Larger Surface Area for Efficient Energy-Storage Performance. *ACS Appl. Energy Mater.* **2018**, *1*, 1567−1574.
(59) Wang, Z.; Tammela, P.; Huo, J.; Zhang, P.; Strømme, M.; Nyholm, L. Solution-processed poly(3,4-ethylenedioxythiophene) nanocomposite paper electrodes for high-capacitance flexible supercapacitors. *J. Mater. Chem. A* **2016**, *4*, 1714−1722.

DOI: 10.1021/acsami.9b03830
ACS Appl. Mater. Interfaces 2019, 11, 16647−16655